Variations of the Solar Acoustic High-Degree Mode Frequencies over Solar Cycle 23

M.C. Rabello-Soares [a], Sylvain G. Korzennik [b], J. Schou [a]

[a] *W. W. Hansen Experimental Physics Laboratory, Stanford University, 455 Via Palou, Stanford, CA 94305, USA*

[b] *Harvard-Smithsonian Center for Astrophysics, 60 Garden St, Cambridge, MA 02138, USA*

Abstract

Using full-disk observations obtained with the Michelson Doppler Imager (MDI) on board the Solar and Heliospheric Observatory (SOHO) spacecraft, we present variations of the solar acoustic mode frequencies caused by the solar activity cycle. High-degree ($100 < \ell < 900$) solar acoustic modes were analyzed using global helioseismology analysis techniques over most of solar cycle 23. We followed the methodology described in details in Korzennik, Rabello-Soares & Schou (2004) to infer unbiased estimates of high-degree mode parameters (see also Rabello-Soares, Korzennik & Schou, 2006). We have removed most of the known instrumental and observational effects that affect specifically high-degree modes. We show that the high-degree changes are in good agreement with the medium-degree results, except for years when the instrument was highly defocused. We analyzed and discuss the effect of defocusing on high degree estimation. Our results for high-degree modes confirm that the frequency shift scaled by the relative mode inertia is a function of frequency and it is independent of degree.

Key words: Sun: helioseismology, Sun: activity, Sun: oscillations

1 Introduction

The correlation between solar acoustic mode frequencies and the magnetic activity cycle is well established and has been substantially studied during the last and current solar cycles (see for example Dziembowski & Goode, 2005, and references therein). The general frequency shift behavior suggests that the perturbation by the solar cycle on the acoustic frequencies occurs very close to the solar surface. The physical mechanism, however, is still a matter of debate, namely whether frequencies are changed directly by the magnetic

field or indirectly through an associated change in the solar structure (like a pressure change). A detailed analysis of the frequency shift characteristics will hopefully help understand its physical origin.

We present here a new analysis of high degree mode frequency shifts over most of solar cycle 23, using a global helioseismology technique. High-degree modes are best suited for studying the frequency shift correlation with the solar cycle since the causing mechanism is believed to be localized near the surface and high-degree modes are also confined to a region near the surface. As a result the frequency shifts for high degree modes are up to an order of magnitude larger than for medium degree modes.

2 Global Helioseismology Analysis of High-Degree Modes

In the traditional global helioseismology data analysis methodology, a time series of full-disk Doppler solar images is decomposed into spherical harmonic coefficients, characterized by its degree (ℓ) and its azimuthal order (m). Each coefficient time series is Fourier transformed, and the order of the radial wave-function (n) gets separated in the frequency domain. However, a spherical harmonic decomposition is not orthonormal over less than the full sphere – *i.e.*, the solar surface that can be observed from a single view point– resulting in what is referred as spatial leakage. At low and intermediate degrees, these leaks are separated in the frequency domain from the target mode and individual modes can be identified and fitted. However, at high degrees, the spatial leaks lie closer in frequency (due to a smaller mode separation) and, at high frequency, they become wider (as the mode lifetimes get smaller), resulting in the overlap of the target mode with the spatial leaks that merges individual peaks into ridges. The characteristics of the resulting ridge (central frequency, amplitude, etc...) do not correspond to those of the underlying target mode. This has so far hindered the estimation of unbiased mode parameters at high degrees.

Our methodology to recover the mode characteristics consists in generating and fitting a sophisticated model of the underlying modes that contribute to the ridge power distribution and deduce the offset between the ridge properties and the underlying target mode (Korzennik, 1998). To do this we need a very good model of the relative amplitude of all the modes that contribute to the ridge, *i.e.* the leakage matrix, which in turn requires a very good knowledge of the instrumental properties. The instrumental characteristics must therefore be very well understood and very precisely measured (see Rabello-Soares, Korzennik & Schou, 2001). Although, the highly successful MDI instrument is responsible for great progresses in our understanding of the Sun, there remain some instrumental effects that there are not well character-

ized and/or not taken into account in the data analysis (Korzennik, Rabello-Soares & Schou, 2004).

We have incorporated most of the known instrumental effects important to the high-degree analysis in our most recent spatial decomposition, introducing one effect at a time to estimate the resulting correction on mode parameters (Rabello-Soares, Korzennik & Schou, 2006). The following known instrumental effects were taken into account in this latest spherical harmonic decomposition, whose results are presented here: (1) the correct instantaneous image scale, (2) the radial image distortion, (3) the effect of a tilt of the CCD with respect to the optical axis, (4) the effective P angle and (5) a correction to the Carrington elements.

Since we are focusing our attention in this paper on changes of mode parameters with epoch, we are primarily concerned with instrumental effects that change over time. Although the MDI instrument has been very stable over the years, continuous exposure to solar radiation has increased the instrument front window absorption resulting in a continuous small increase of the instrument best focus. Moreover the change of the front window temperature due to the satellite orbit around the Sun also adds a small annual variation. The instrument has however an adjustable focus with 9 possible positions [1] chosen to best suit the science team needs, resulting unfortunately in abrupt jumps every time that it is changed. These changes are responsible for the largest variations. The best focus is periodically and empirically determined from intensity images taken with different focus positions (Kuhn et al., 2004). The change in the image scale resulting from a change in focus was shown to be an important effect (Korzennik, Rabello-Soares & Schou, 2004) and it is taken care in the analysis presented here. However, the effect of the amount of defocus was not taken into account. A preliminary analysis indicated that it has a small effect on the frequencies (Korzennik, Rabello-Soares & Schou, 2004); we have further studied its influence on the ridge frequency.

3 Description of the Data Set Used

Full-disk Dopplergrams, acquired by the MDI instrument while operating in its $4''$ resolution mode, were used for this analysis. The MDI instrument is operated in this mode, known as the *Dynamics Program*, every year for two to three months, when the required telemetry bandwidth is available. The spherical harmonic decomposition of these Dopplergrams was computed for every tenth ℓ between 100 and 900, and the resulting time series Fourier transformed in shorter segments (as described in Korzennik, Rabello-Soares & Schou, 2004,

[1] One focus step corresponds to approximately a third of a wave

namely 4096 minutes or 2.8 days long) whose power spectra were averaged to produce an averaged power spectrum [2] with a low but adequate frequency resolution to fit the ridge while reducing the realization noise. Table 1 lists the properties of each epoch included in this study. The peaks in each (ℓ, m) spectra were then fitted with asymmetric Lorentzian profiles and the $2\ell + 1$ frequencies for each (n, ℓ) multiplet expanded in terms of Clebsch-Gordan coefficients up to a_6 (see Korzennik, Rabello-Soares & Schou, 2004, for details).

We also compare our results (hereafter referred to as the high-ℓ set) to results obtained by one of us using the MDI *Structure Program*. In this mode the original Dopplergrams are convolved, on board the MDI instrument, with a Gaussian and subsampled on a 200×200 grid, thus reducing the telemetry requirements but also limiting the spatial resolution to modes with degree $\ell < 300$. The data sets consist of 72-day-long time series that partially overlap with the *Dynamics* periods (see Table 1). The central frequencies and the splitting coefficients were determined directly from fit to symmetric Lorentzians (Schou, 1999). Although the instrumental effects listed in Section 2 were not taken into account here, their effects are much smaller because the spatial leaks are well separated from the target mode (Schou & Rabello-Soares, 2001).

The coverage of both analyses is illustrate in an $\ell - \nu$ diagram in Fig 1. Note that there is a small overlap in the coverage of both methods. Indeed, by degrading the frequency resolution one can merge resolved modes into a smooth ridge and apply the ridge fitting methodology developed for high degrees to intermediate degrees.

The MDI data analyzed here, see Table 1, covers much of solar cycle 23, as illustrated in Fig. 2. The average solar UV spectral irradiance (given by the NOAA Mg II core-to-wing ratio) relative to the 30-day running mean maximum of solar cycle 23 (reached in January 2002) for each epoch is listed in Table 1. That table also lists the average defocus of the MDI images during each *Dynamics* epoch, in units of MDI focus steps. Early on (1996 to 1998) the instrument was set to a large defocus (up to 2.5 focus steps), while later on the instrument was set to be nearly on focus (*i.e.*, a defocus of 0.5 focus steps in average).

4 Analysis of the Frequency Shift

Figure 3 shows mode frequency differences between 2002 and 2005, namely between high and moderate activity epochs respectively, resulting from medium

[2] Henceforth the number of averaged spectra varies with epoch, from 12 segments in 2003, to 32 in 1997.

and high degree determinations. The frequency shifts for each order, n, scale as a power law with the quantity ν/L (where $L = \ell + 0.5$, a good proxy of the mode inner turning point), and can be described in a first approximation by $\delta\nu_{n,\ell} \propto I_{n,\ell}^{-1}$, where $I_{n,\ell}$ is the mode inertia (as first noticed by Libbrecht & Woodard, 1990).

For the observational periods where the MDI instrument was set to a large defocus (1996 to 1998), our measured frequency shifts for high-ℓ do not agree with results from medium-ℓ. The defocus has a substantial effect on the ridge central frequencies, contrary to our initial expectations. The resulting instrumental point spread function (PSF) is affected and the effect of a varying PSF has not yet been incorporated in our analysis, therefore we will not include these epochs in our analysis of changes of mode parameters with the solar cycle.

Figure 4 shows the correlation between the frequency shift and the solar activity index variation (given by the solar UV irradiance) for four modes with frequency around 3 mHz at high degree ($\ell = 200, 400, 600$ & 800) for the 1999 to 2004 epochs with respect to the 2005 epoch. We have fitted, using a weighted least-squares minimization, the frequency shift to the solar index variation, assuming a linear relationship with a zero intercept (solid line). This fit was performed for each (n, ℓ) mode of the medium and high-ℓ sets separately, resulting in a total of 1468 and 423 regression fits respectively.

We also computed correlations between the frequency shift and the Magnetic Plage Strength Index (Mt. Wilson Observatory), the solar radio 10.7 cm flux (National Research Council of Canada) and the sunspot number (SIDC, RWC Belgium) using the high-ℓ set. The magnetic index gives similar Pearson correlation coefficients as the UV flux while the radio flux coefficients are slightly smaller (by a few percent). The sunspot number correlation coefficients are also similar to those for the UV flux but only for frequencies around 3 mHz, their correlation coefficients increase as the frequency decreases, by some 20%.

The frequency shift between solar maximum and minimum can be estimated by multiplying the slope of the linear fit (solid line in Fig. 4) by the corresponding solar index variation. We used the 30-day running mean values to estimate the minimum and maximum, reached in March 1996 and January 2002 respectively. We rejected modes whose Pearson correlation coefficient is smaller than 0.8, or whose slope uncertainty is larger than 20% and only fitted modes for which we have estimates for at least five of the six epochs. This estimated minimum-to-maximum frequency shift, $\delta\nu^e$, incorporates information from all the data sets (1999 to 2005) in a consistent way, decreasing ipso facto the uncertainties.

The frequency shift increases sharply with frequency and degree. Although

several authors multiply the frequency shift by the mode inertia to remove its ℓ dependence, we found, as others have at lower and medium-ℓ (Chaplin et al., 2001), that the mode inertia normalized by the inertia of a radial mode of the same frequency gives a better agreement between the medium and high-ℓ set shifts, as shown in Fig. 5. The estimated minimum-to-maximum frequency shifts can be described according to a simple power law, *i.e.*:

$$\delta\nu^{e}_{n,\ell} = C_{\gamma}\ \frac{(\nu_{n,\ell})^{\gamma}}{Q_{n,\ell}} \tag{1}$$

where $Q_{n,\ell}$ is the relative mode inertia, *i.e.*:

$$Q_{n,\ell} = \frac{I_{n,\ell}}{I_{n,0}} \tag{2}$$

and $I_{n,\ell}$ is the mode inertia calculated from Christensen-Dalsgaard's model S (see Christensen-Dalsgaard et al., 1996). The frequency dependence of the frequency shift scaled by $Q_{n,\ell}$ shows the relative importance of the contribution from the surface layers in relation to the the solar interior (Christensen-Dalsgaard et al., 1989).

We fitted Eq. 1 to estimate γ, using a weighted least-squares minimization, as illustrated in Fig. 5. For p modes, we found very similar results for the medium- and high-ℓ sets: $\gamma_p = 3.64 \pm 0.02$ (dashed) and $\gamma_p = 3.62 \pm 0.04$ (solid) respectively. Note that in the lower panel there is a step in the frequency shift around 2.3 mHz and only modes with $\nu \geq 2.5$ mHz were included in the fitting of the medium-ℓ set mentioned above. Despite the step, modes with $\nu < 2.23$ mHz show a similar value of γ as for $\nu \geq 2.5$ mHz: $\gamma_p = 3.5 \pm 0.3$ (dotted and dashed line). It is interesting to point out that the height of the upper turning point decreases very fast with mode frequency for $\nu < 2.3$ mHz (see Fig.2 in Chaplin et al., 2001). The f modes for the high-ℓ set are strongly correlated with the solar cycle (see lower right panel in Fig. 4) and exhibit a behavior similar to the p modes with a positive γ_f but with a $\gamma_f = 1.6 \pm 0.2$ (dotted line in the upper panel of Fig. 5), less than half of γ_p, which could be an indication that different physical effects are responsible for the solar-induced frequency shifts (see Dziembowski & Goode, 2005). There are no f modes in the medium-ℓ set with a correlation higher than 0.8 for comparison.

Chaplin et al. (2001) scaled the frequency shift by the mode inertia, *i.e.*:

$$\delta\nu^{e}_{n,\ell} = C_{\alpha}\ \frac{(\nu_{n,\ell})^{\alpha}}{I_{n,\ell}} \tag{3}$$

and estimated α for $4 < \ell < 150$ using GONG data. They found $\alpha \approx 0$ for $1.6 < \nu < 2.5$ mHz and $\alpha = 1.92 \pm 0.03$ for $2.5 < \nu < 3.9$ mHz. To compare

our results, we multiplied our fit, $C_\gamma\ \nu^\gamma$, by $I_{n,0}$ and fitted the function $C_\alpha\ \nu^\alpha$. Our results using MDI medium and high-degree modes agree well in the high-frequency range, *i.e.*: $\alpha = 1.97 \pm 0.02$. However, MDI medium-ℓ modes exhibit a negative slope $\alpha = -3.05 \pm 0.01$ for $\nu < 2.5$ mHz. Note that $\log(\delta\nu^e_{n,\ell}\ I_{n,\ell})$ display a quadratic dependence on $\log(\nu_{n,\ell})$, with an inflection point at 2.59 mHz as shown in Fig. 6. This minimum in the frequency shift scaled by the mode inertia $I_{n,\ell}$ is also seen in Figures 4 and 5 in Howe, Komm & Hill (2002).

The solar-cycle correlation coefficients decrease sharply for modes with $n > 6$ and frequencies larger than ~ 4.8 mHz, some of them becoming even negative. However, these "anti-correlation" coefficients are not large enough to draw any conclusion other than these modes present no significant correlation with the solar cycle.

5 Influence of Image Defocus on the Frequency Shifts

As mentioned before, the frequency shifts for 1996 to 1998 are biased due to the change in the amount of defocus. To estimate the resulting bias, we computed the correlation versus the solar activity index and estimated the minimum-to-maximum frequency shift, $\delta\nu^e$, as described in the previous section, but using only these three epochs. These biased frequency shifts remain strongly correlated with the solar cycle, but the result is affected by the defocus, as illustrated in Fig. 7. The differences are substantial for $n < 4$ and for $\ell > 600$. Note that the change in the amount of defocus with respect to 2005 averages to 0.16 (in focus steps) for the later years (1999 to 2004), while that same quantity averages to 1.77 for the early years (1996 to 1998), namely an order of magnitude larger. The remaining frequency bias due to change in defocus could be as large as the frequency shift due to solar activity.

We can not discard the fact that the frequency shifts in Fig. 5 using 1999 to 2005 may have some significant, although very small, bias due to variations in the defocus between the data sets (*i.e.* 1999 to 2004 with respect to 2005). The instrumental PSF must be taken into account in the analysis at least for data sets taken when the instrument was out of focus.

6 Conclusions

We analyzed the variation of the solar acoustic frequencies during solar cycle 23 using medium and high degree modes. Our high-ℓ mode analysis incorporates most observational and instrumental effects that affect specifically high-ℓ in

the spherical harmonic decomposition to produced unbiased mode estimates from ridge fitting.

The frequency shift scales very well with the mode inertia normalized by the inertia of a radial mode of the same frequency and follows Eq. 1, where $\gamma = 3.63 \pm 0.02$ for p modes using medium-ℓ (MDI Structure Program) and high-ℓ (MDI Dynamics Program) data and $\gamma = 1.6 \pm 0.2$ for the f modes, which exhibit a different behavior.

The frequency variation does not appear correlated with solar activity for frequencies larger than ~ 4.8 mHz. There is also an abrupt step in the scaled frequency shift for frequencies smaller than ~ 2.3 mHz.

We also analyzed the effect of defocusing on the high-ℓ frequency determination. This is particularly important for the first three years of MDI observations when the instrument was set to a substantial defocus. This has a larger impact on modes with $n < 4$ and $\ell > 600$. Further progress will be achieved by including a time varying PSF in the high-ℓ global helioseismology analysis.

7 Acknowledgments

The Solar Oscillations Investigation (SOI) involving MDI is supported by NASA grant NNG05GH14G at Stanford University. SOHO is a mission of international cooperation between ESA and NASA. SGK is supported by NASA grant NNG05GD58G. NOAA Mg II Core-to-wing ratio data are provided by Dr. R. Viereck, NOAA Space Environment Center. The solar radio 10.7 cm daily flux (2800 MHz) have been made by the National Research Council of Canada at the Dominion Radio Astrophysical Observatory, British Columbia. The International Sunspot Number was provided by SIDC, RWC Belgium, World Data Center for the Sunspot Index, Royal Observatory of Belgium. This study includes data from the synoptic program at the 150-Foot Solar Tower of the Mt. Wilson Observatory. The Mt. Wilson 150-Foot Solar Tower is operated by UCLA, with funding from NASA, ONR and NSF, under agreement with the Mt. Wilson Institute.

References

Chaplin, W. J., Appourchaux, T., Elsworth, Y., Isaak, G. R., New, R., The phenomenology of solar-cycle-induced acoustic eigenfrequency variations: a comparative and complementary analysis of GONG, BiSON and VIRGO/LOI data, 2001, MNRAS 324, 910-916.

Christensen-Dalsgaard, J., Thompson, M. J., Gough, D. O., Differential asymptotic sound-speed inversions, 1989, MNRAS 238, 481-502.

Christensen-Dalsgaard, J., Dappen, W. et al., The Current State of Solar Modeling, 1996, Science 272, 1286-1292.

Dziembowski, W.A. & Goode, P.R., Sources of oscillation frequency increase with rising solar activity, 2005, Ap.J. 625, 548-555.

Howe, R., Komm, R.W., & Hill, F., Localizing the solar cycle frequency shifts in global p-modes, 2002, Ap.J. 580, 1172-1187.

Korzennik, S. G., Observational Analysis of Asymmetries in Velocity and Intensity Power Spectra, 1998, ESA SP-418, p. 933-938.

Korzennik, S. G., Rabello-Soares, M. C., & Schou, J., On the determination of Michelson Doppler Imager high-degree mode frequencies, 2004, Ap.J., 602, 481-515.

Kuhn, J. R., Bush, R. I., Emilio, M. & Scherrer, P. H., On the constancy of the solar diameter II, 2004, Ap.J. 613, 1241-1252.

Libbrecht, K. G., Woodard, M. F., Solar-cycle effects on solar oscillation frequencies, 1990, Nature 345, 779-782.

Rabello-Soares, M. C., Korzennik, S. G. & Schou, J., The determination of MDI high-degree mode frequencies, 1999, ESA SP-464, p.129-136.

Rabello-Soares, M. C., Korzennik, S. G. & Schou, J., High-degree mode frequencies: changes with solar cycle, 2006, ESA SP-624, in press.

Schou, J., Migration of zonal flows detected using Michelson Doppler Imager f-mode frequency splittings, 1999, Ap.J., 523, L181-184.

Schou, J. & Rabello-Soares, M. C., An Investigation of Systematic Errors in MDI Mode Parameters, 2001, American Geophysical Union, Spring Meeting 2001, SP31A-24

Table 1
Observational periods, relative average solar active index and average defocus.

Year	Starting Date *Dynamics* [Month/Day]	Duration *Dynamics* [days]	Solar Index rel. to max. [in %]	Average Defocus	Starting Date *Structure* [Month/Day]
1996	05/23	63	2 ± 3	2.07 ± 0.07	05/01
1997	04/13	93	5 ± 3	2.53 ± 0.07	04/26
1998	01/09	92	20 ± 7	1.75 ± 0.05	02/08
1999	03/13	77	40 ± 13	0.1 ± 0.4	02/03
2000	05/27	45	69 ± 11	0.45 ± 0.02	04/10
2001	02/28	90	61 ± 14	0.57 ± 0.04	01/23
2002	02/23	72	80 ± 8	0.77 ± 0.05	03/31
2003	10/18	38	51 ± 17	0.92 ± 0.01	10/28
2004	07/04	65	36 ± 11	0.2 ± 0.1	08/11
2005	06/25	67	30 ± 9	0.34 ± 0.02	05/26

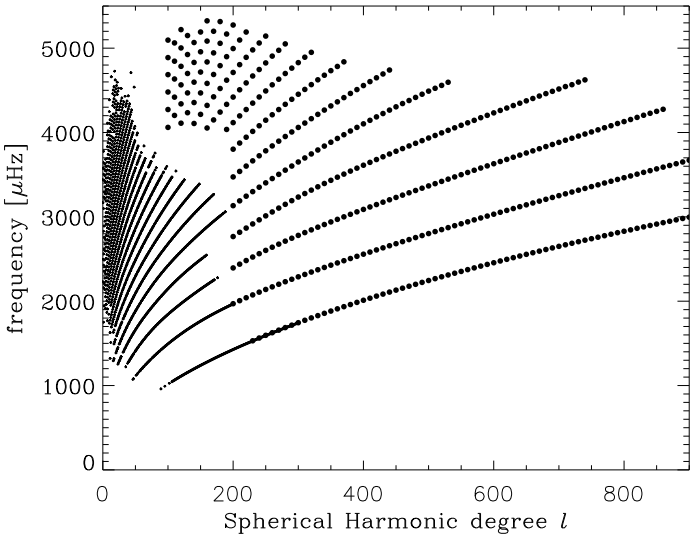

Fig. 1. Coverage, in an $\ell - \nu$ diagram, of the medium-ℓ (crosses) and high-ℓ (circles) set for 1996. The coverage is very similar for all epochs. Modes with $\ell < 200$ and $\nu < 4$ mHz may not completely overlap with their spatial leaks and were excluded from the present high-ℓ analysis.

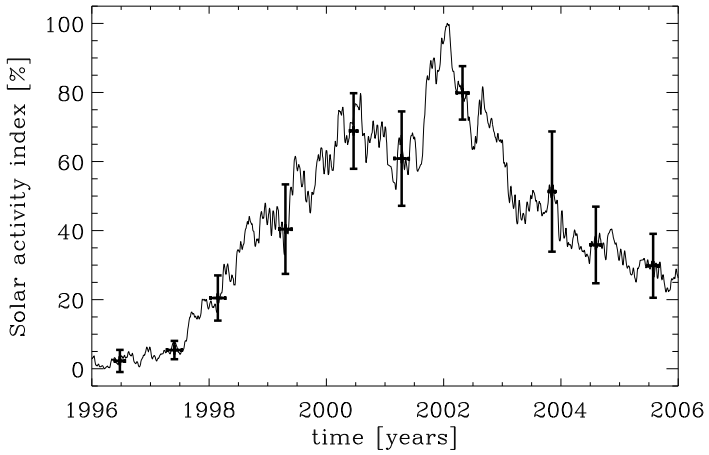

Fig. 2. Solar UV spectral irradiance (given by the NOAA Mg II core-to-wing ratio) 30-day running mean relative to its maximum during solar cycle 23 (line) and its average for each epoch.

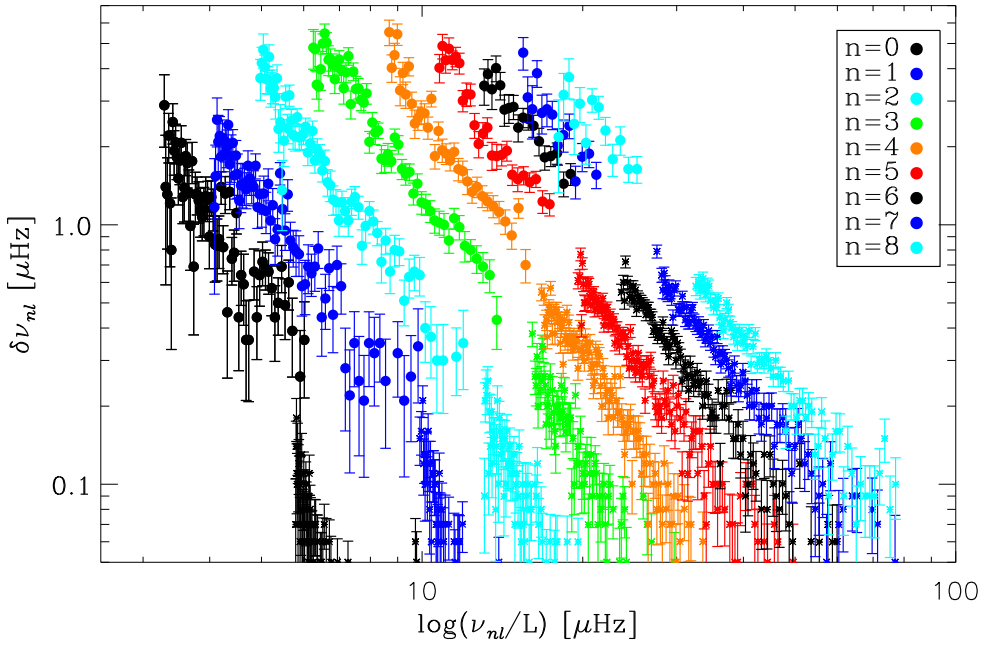

Fig. 3. Differences between the mode frequencies as observed in 2002, near solar maximum, and in 2005, during moderate activity. Only modes with $n = 0$ to $n = 8$ are plotted (evens in black, odds in grey). The medium-ℓ set is indicated by stars (lower part of the plot) and high-ℓ set by circles (upper part).

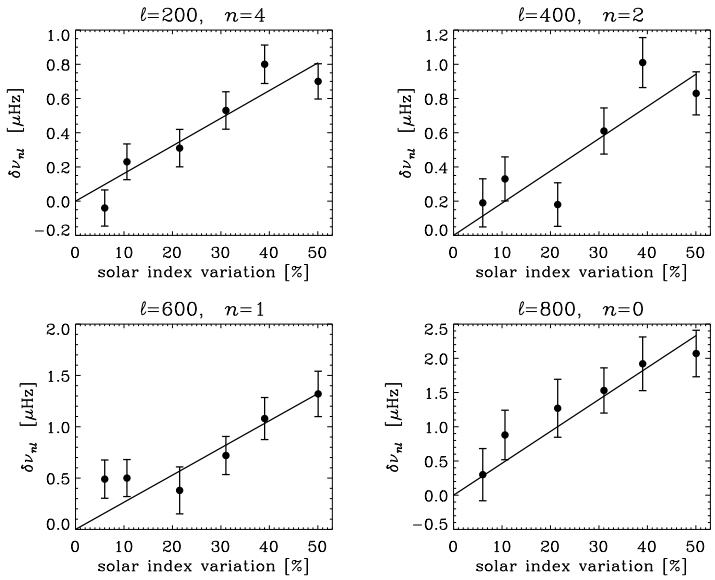

Fig. 4. Examples of correlation between the frequency shift and the solar cycle for six epochs (1999 to 2004) with respect to 2005 for four high-ℓ modes with different degree and order but similar frequency ($\sim$ 3 mHz). The error bars are the standard deviation of the fitted frequencies. The straight line is a weighted least-squares fit to the data, keeping the intercept to zero.

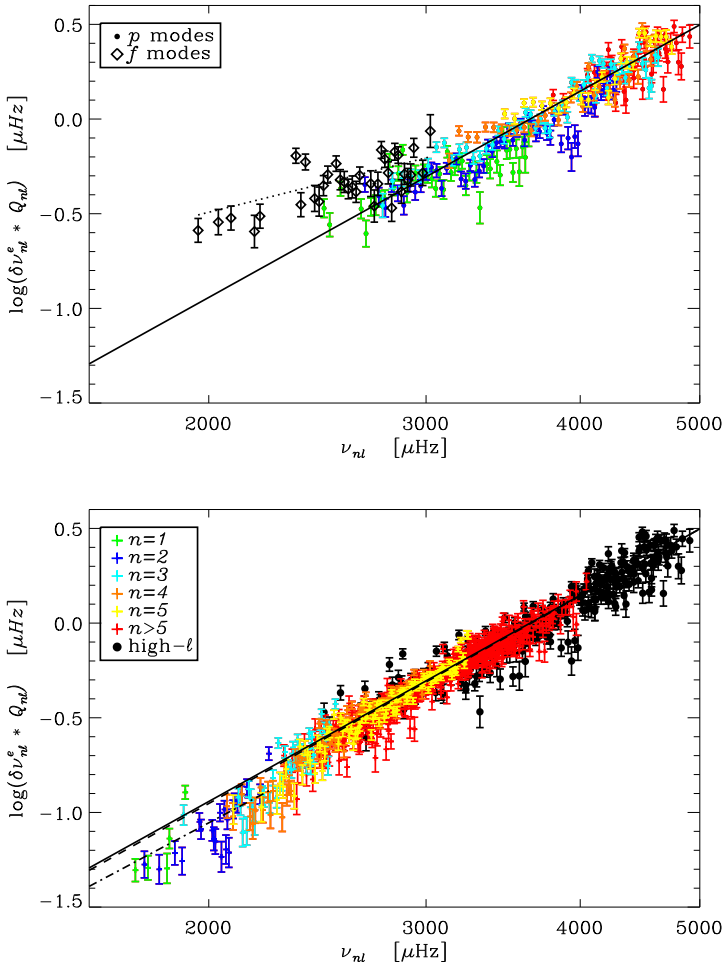

Fig. 5. Minimum-to-maximum frequency shift multiplied by the normalized mode inertia as a function of frequency. The upper panel shows only the high-ℓ set and, in the lower panel, the high-ℓ p modes are indicated in black (circles) and the medium-ℓ p modes in gray (crosses).

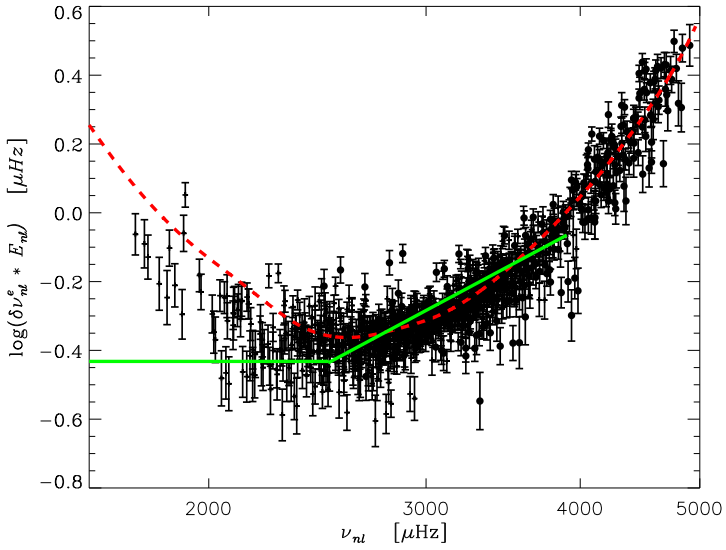

Fig. 6. Minimum-to-maximum frequency shift multiplied by the mode inertia as a function of frequency. The medium and high-ℓ p modes are represented by crosses and circles respectively. The dashed line corresponds to the dashed line in the lower panel of Fig. 5. The solid line is given by Eq. 3 using the values estimated by Chaplin et al. (2001): $\alpha = 0$ for $1.6 < \nu < 2.5$ mHz and $\alpha = 1.92$ for $2.5 < \nu < 3.9$ mHz; the fitted values for C_α were not given by the authors hence ad hoc values were used.

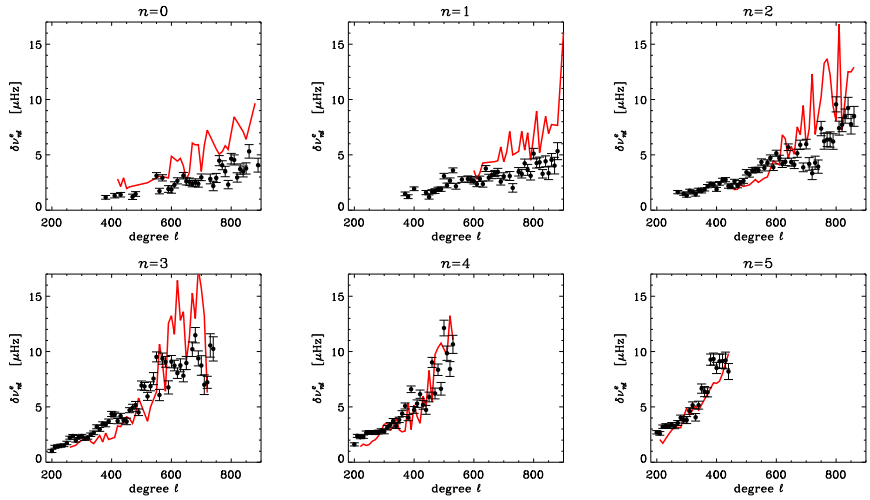

Fig. 7. Minimum-to-maximum frequency shift estimated using 1999 to 2004 data sets with respect to 2005 (black circles - same as in Fig. 5) and using 1996 to 1998 data sets with respect to 2005 (solid line). Note that, for the later, there is a larger scatter and the standard deviation is also larger (not plotted for clarity) due to the small number of available epochs. Modes whose Pearson correlation coefficient is smaller than 0.8 or whose slope uncertainty is larger than 20% were excluded from the plot.